RESEARCH ARTICLE

Applied Polymer WILEY

Self-healing efficiency of cinnamaldehyde-crosslinked soy protein resins with elongated soy protein microcapsules

Vuthtyra Yong | Anil N. Netravali

Department of Fiber Science & Apparel Design, Cornell University, Ithaca, New York, USA

Correspondence

Anil N. Netravali, Department of Fiber Science & Apparel Design, Cornell University, Ithaca, New York 14853, USA. Email: ann2@cornell.edu

Abstract

Self-healing green thermoset soy protein isolate (SPI) based resins, crosslinked with cinnamaldehyde (CA), were developed. Self-healing was achieved using elongated microcapsules (MCs) as against spherical MCs that have been used in most earlier studies. MCs containing SPI solution as healant within poly(d,llactide-co-glycolide) shells were prepared using Water-in-oil-in-water (w/o/w) emulsion solvent evaporation (ESE) technique. Process parameters such as sodium tripolyphosphate (STP) and poly(vinyl alcohol) (PVA) concentrations and stirring speed were optimized to obtain elongated MCs. The average aspect ratio of MCs was over four. SPI resins crosslinked with 10% CA (10%CA-SPI) increased Young's modulus and fracture stress by 54% and 87%, respectively, compared with their noncrosslinked counterpart. The resins containing 15% elongated MCs (15%MC-10%CA-SPI) showed self-healing efficiencies of over 42% in fracture stress and about 35% in toughness recovery, after 24 h of healing. Improvement in self-healing can be attributed to the high aspect ratio of the MCs that increases the probability of MCs being in the path of the microcracks and releasing the healant. Elongated MCs also contain higher amount of healant than spherical ones of same diameter. Self-healing resins and composites can not only help prevent their premature failure but also improve their performance as well as service life and safety.

KEYWORDS

biopolymers and renewable polymers, green composites, mechanical properties, proteins, self-healing

1 | INTRODUCTION

Synthetic polymers have been used in numerous day-to-day applications. However, our extreme dependence on them has created significant problems for humans, the environment, and the planet. As most synthetic polymers originate from petroleum, a nonrenewable resource, their growing demand has contributed to unsustainable petroleum consumption. At the current depletion rate, recent studies have predicted that the current petroleum reserves may not last beyond the next 50–60 years.^{1–3}

Aside from the sustainability issue, most synthetic polymers and composites made using them end up in landfills while only a small fraction is powdered for use as filler or incinerated after their service life. While landfilled plastic waste uses scarce land and pollutes the land, water, and the entire ecosystem, incineration of plastic waste generates enormous amounts of carbon dioxide and other toxic gases that pollute the air.

Over the past 3–4 decades, there have been many studies that have tried to address such environmental and sustainability issues. As a solution, some researchers

have studied a broad variety of partially to fully biodegradable resins and composites derived from yearly renewable natural resources such as plants.^{8,9} Plantbased polymers such as proteins and starches, are now considered as possible replacements for petroleum-based resins since they are abundantly available, economical, fully sustainable, and biodegradable. 3,8,10 These natural polymers contain building blocks that mimic synthetic structures and can be made into functional materials having remarkable performance. 11 Other researchers, however, have sought novel solutions to prolong the service life of existing materials. 12,13 Cracks and microcracks are the main culprits for premature failure of polymers and composites when they operate under extreme environments such as high stress/strain, cyclic loading, humidity, or oxygen-rich conditions. One of the effective solutions to prevent the microcracks from growing to catastrophic levels is through autonomous self-healing, which allows materials to recover from damages at the microstructural level. 1-3,8,14,15 This self-healing characteristic not only extends the life of the materials but also enhances the safety of the products as well as the users.

Soy protein isolate (SPI), derived from defatted soybeans, has been used in many applications, including adhesives, plastics, binders, resins, and composites. 2,9,16,17 SPI contains about 90% protein with a broad range of molecular weights from 8 kDa to 600 kDa. 10 These protein or polypeptide molecules are composed of 18 different amino acids. 18 Some of the amino acids contain polar functional groups, such as amine, carboxyl, and hydroxyl groups, that are capable of reacting with each other under the right conditions. Under oxidative conditions, for example, sulfur-sulfur bonds and dehydroalanine groups are formed at cysteine and lysine amino acids, respectively. Lysine and arginine amino acids containing amine groups can form amide crosslinks when heated, with amino acids such as glutamic and aspartic acids that contain carboxyl groups. SPI-based resins generally exhibit good strength, but they are highly hygroscopic due to the presence of these polar functional groups. 19 Nonetheless, researchers have successfully crosslinked soy protein-based resins, using external crosslinkers, to enhance their mechanical and thermal properties while minimizing moisture absorption. Many commercial aldehyde crosslinkers, including glyoxal, glutaraldehyde, and formaldehyde, have been studied and commonly applied in wood-based composite materials and resins to enhance their strength and water resistance. 20-24 Chabba and Netravali found that crosslinking soy protein concentrate-based (SPC) resins with 10% (w/w) glutaraldehyde increased the fracture stress and Young's modulus by 20% and 35%, respectively, along with improvement in moisture resistance.²⁵ When modified with 5% (w/w) formaldehyde, SPI

films significantly increased tensile strength by about 20% and Young's modulus by 15%.²⁶ Despite improved mechanical properties, the inherent toxicity and carcinogenicity of these crosslinkers have limited their use in biobased green applications. In contrast, cinnamaldehyde (CA), a naturally occurring aromatic aldehyde compound from cinnamon barks, has shown promising crosslinking effects, especially with wheat gliadins and Karanja proteins.^{27,28} CA is also well-known for its antimicrobial property, providing excellent protection against microbes and insects, and hence increases the durability of protein-based resins and composites.²⁸

The incorporation of self-healing property into conventional materials has been studied for many decades. The earliest self-healing studies on autonomous self-healing polymeric materials were conducted about 50 years ago.²⁵ Since then, the self-healing property has been expanded to materials such as metals, ceramics, concretes, composites, biobased materials, and so forth.³⁰ Self-healing systems discussed in the open literature primarily include microcapsule (MC)-based, microvascular, click-chemistry, hydrogen bonding, and thermal-activation.^{2,31-34} The MC-based system is by far the most preferred method due to the ease of processing, better MC dispersion methods, and more uniform selfhealing for the host materials. The microcapsules (MCs) consist of two main components: polymer shells and healing agents (healants) that are encapsulated in the shells.^{2,3} When microcracks propagate in the host materials, MCs in their path fracture, releasing the healant. Healants, mostly in liquid form, flow easily inside the crack and solidify. bridging the two surfaces. Synthetic polymers such as epoxy, ^{35–37} dicyclopentadiene, ^{38,39} polydimethylsiloxane, ^{40,41} glycidyl methacrylate, 42,43 isocyanate, 44,45 and so forth, have been the most commonly used healing agents. Recently, a few studies have shown successful use of green healing agents, such as soy protein^{1,2,14} and waxy maize starch (WMS)^{3,8} in self-healing green thermoset composites/resins.

One of the most common techniques to fabricate microcapsules is emulsion solvent evaporation (ESE). Although there are many reports of using various types of emulsion systems, the water-in-oil-in-water (W/O/W) emulsion system is arguably the most successful and efficient method for MC preparation.3 Kim and Netravali reported successful encapsulation of SPI or WMS inside poly(lactic-co-glycolic acid) (PLGA) shell via a w/o/w ESE technique.^{8,46} With the processing condition of 1% PLGA as the dispersed phase, 5% poly(vinyl alcohol) (PVA) as the continuous phase, and 10,000 rpm of stirring speed, they were able to achieve 85% SPI encapsulation efficiency and 34.3% protein loading.46 The SPI-based thermoset resin containing 15 wt% MCs demonstrated a self-healing efficiency of 53% after 24 h of healing time. Shi and Netravali employed a similar

method with some modifications to fabricate PLGA MCs with SPI containing bacterial cellulose (BC).¹⁴ With 20 wt% of SPI-BC/PLGA MCs, SPI resins showed a self-healing efficiency of about 45% in strength and 59% in toughness recovery.

Elongated MCs, because of their higher aspect ratios, are thought to have higher probability of being in the microcrack path and fracturing than the conventional spherical MCs, thus, being more effective in bridging cracks and resulting in higher self-healing efficiency.^{3,14} In addition, elongated MCs can also contain more healant compared to spherical MCs of same diameter. However, preparation of elongated MCs is not as simple as spherical ones. The primary goals of this study were to successfully prepare elongated MCs and characterize their self-healing efficiency. Many elongated MC fabrication techniques discussed in the literature, such as heatstretching of spheres,⁴⁷ template-based molding,^{48,49} microfluidic techniques, 50 and so forth, suffer from shell degradation and leaching and can be expensive and complicated to setup. Nevertheless, some efficient and straightforward fabrications of ellipsoidal capsules loaded with various therapeutics have been reported. 51,52 Safari et al. used ESE in the presence of surface-active molecules such as sodium tripolyphosphate (STP), Trizma base, and sodium metaphosphate.⁵³ They showed that with 2% STP, 2% PVA, and 2500 rpm stirring, more than 65% yield of PLGA capsules with aspect ratio of five can be attained.

In the present study, SPI-based self-healing green thermoset resins were developed that can address the environmental and sustainability concerns arising from the ubiquitous consumption of synthetic polymers. The effect of CA crosslinking on the tensile properties of SPI resins was investigated. Self-healing CA crosslinked thermoset SPI (CA-SPI) resins were prepared by incorporating elongated MCs (fabricated via Safari's modified two-step emulsion method). The self-healing efficiencies of the composite resins were evaluated.

2 | EXPERIMENTAL

2.1 | Materials

SPI, PROFAM[®] 974, was provided by Archer Daniels Midland Co. (Decatur, IL). Sodium hydroxide pellets, sodium tripolyphosphate, and trans-CA (≥98%) were purchased from VWR (Rochester, NY). Poly(vinyl alcohol) (PVA, average MW 89–98 K, 99% hydrolyzed), rhodamine B, D-sorbitol (≥98% purity), hydrogen chloride solution, and Bradford reagent (for 0.1–1.4 mg/mL protein) were purchased from Sigma Aldrich Chemical

Co. (St. Louis, MO). Sodium dodecyl sulfate (SDS) and dichloromethane (DCM) were purchased from Fisher Chemical (Fair Lawn, NJ). Poly(D, L-lactide-co-glycolide) (50:50) (PLGA, Ester terminated, Inherent viscosity of 0.65 dL/g in HFIP) was purchased from LACTEL Absorbable Polymers (Birmingham, AL).

2.2 | Preparation of elongated SPI-PLGA microcapsules

Elongated SPI-PLGA microcapsules were prepared using the w/o/w ESE technique described earlier. 1,2,8,46,53 The schematic of the process is shown in Figure 1. The core aqueous phase was prepared by mixing 1 g of SPI in 10 mL of deionized (DI) water followed by 4 M NaOH solution to obtain a pH of 12. The aqueous solution was stirred at 350 rpm and 80°C for 30 min to ensure complete dissolution of SPI. The aqueous solution was then emulsified with 1% PLGA in 30 mL of DCM using a vortex mixer (BenchMixer) at maximum speed for 3 min, as shown in Figure 1a. The prepared w/o emulsion was injected at 1 mL/min rate into 100 mL of (2% PVA, 0.04 M STP) solution while being stirred at 700 rpm, as shown in Figure 1b. The injection process was carried out using a Harvard apparatus fusion pump, where two 10 mL syringes, each attached to a 25-gauge hypodermic needle, were placed side by side. To ensure full evaporation of DCM to form the shell wall, the final solution was stirred at 700 rpm for 3 h. The MCs were collected after centrifugation at 3000 rpm for 10 min. The obtained MCs were washed three times with DI water, filtered, and then freeze-dried at -50° C for 24 h.

2.3 | Preparation of CA-SPI and MC-CA-SPI green thermoset resins

To prepare CA crosslinked CA-SPI resins, SPI powder (15 g) was mixed with 150 mL of DI water, followed by 4 M NaOH solution to achieve a pH of 11. The SPI solution was stirred at 300 rpm and 80°C for 15 min. Predetermined amounts of CA (0, 5, 8, or 10 wt% based on SPI powder) and D-Sorbitol (10 wt% based on SPI powder) were then added to the mixture and stirred for another 30 min. Commonly, 8% CA is enough for proper crosslinking of resin. At 10% CA there is slightly extra crosslinker in the resin that allows crosslinking of the released healant. The resin mixture was poured onto a Teflon® coated sheet and allowed to dry in an air-circulating oven at 40°C for 48 h. The partially cured/dried resin sheets were hot-pressed at 90°C under a pressure of 0.45 MPa for 10 min to obtain 2-mm-thick cured SPI resin sheets.

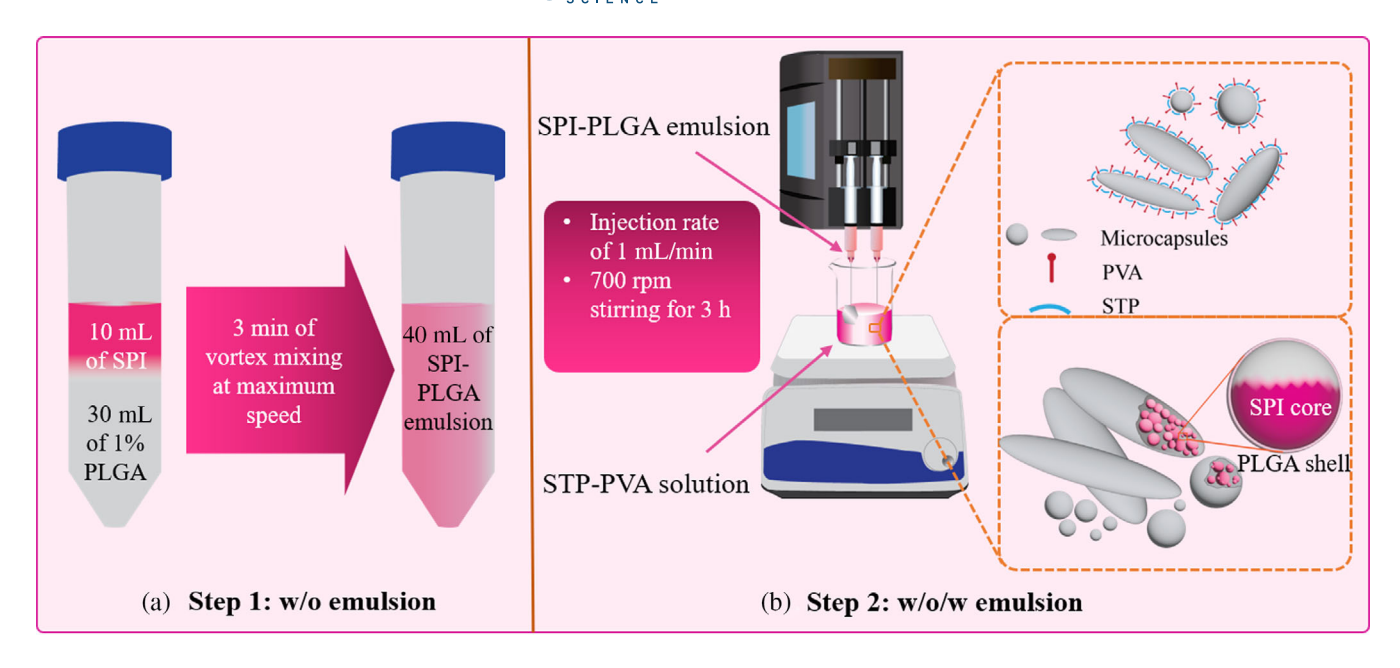


FIGURE 1 Schematic of (a) w/o SPI-PLGA emulsion and (b) w/o/w SPI-PLGA-PVA emulsion solvent evaporation (ESE) process to produce elongated microcapsules. PLGA, poly(lactic-*co*-glycolic acid); PVA, poly(vinyl alcohol); SPI, soy protein isolate; STP, sodium tripolyphosphate. [Color figure can be viewed at wileyonlinelibrary.com]

Similarly, all MC-loaded CA-SPI (MC-CA-SPI) resin sheets were prepared as per the CA-SPI resin procedure mentioned earlier. However, predetermined amounts of elongated MCs (5, 10, or 15 wt% based on SPI) were mixed in the SPI solution and stirred for 10 min before adding (10 wt%) CA and (10 wt%) D-sorbitol. Both types of resin sheets, with and without MCs, were conditioned at 21°C and 65% RH for 72 h before characterization.

2.4 | Characterization of the elongated microcapsules

Zeiss Gemini 500 scanning electron microscope (SEM) was used to investigate the size, shape and topography of the fabricated MCs. To obtain SEM images, a drop of 1% (w/v) MC suspension in DI water was put on a piece of a silicon wafer to dry. The wafer was mounted on a conductive carbon tape glued to the SEM metal stub. The wafer with the MCs was then gold-coated for imaging. Diameters and lengths of the elongated MCs were determined by randomly selecting MCs from two SEM images and measured using ImageJ software. Aspect ratios of individual MCs were calculated using their diameters and lengths.

MCs that contained SPI slurry stained with 0.5% rhodamine B were examined using a confocal laser scanning microscope (CLSM) (Zeiss LSM 710) equipped with 25 mW argon and HeNe lasers (excitation at 514 nm) and $63\times$ oil immersion lens. Both transmission and

fluorescent CLSM images were obtained to analyze the internal structures of the MCs and to confirm the presence of the SPI in the MC cores. The surface chemical compositions of MCs were studied using attenuated total reflectance Fourier-transform infrared (ATR-FTIR) (Magna 560, Nicolet Instrument Technologies, Fitchburg, WI, USA) spectroscopy.

2.5 | Determination of encapsulation efficiency and protein loading in MCs

Protein loading in MCs was determined using the protocol developed by Kim and Netravali, with some modifications. 10 mg of freeze-dried MCs containing SPI was added to 10 mL of 0.1 M NaOH solution containing 5% (w/v) SDS. The solution was stirred at 300 rpm overnight or until it turned transparent. The solution was then centrifuged for 10 min at 5000 rpm to remove the insoluble residues. The standard curve was constructed from an array of pure SPI references (2, 5, 7.5, 10, and 14 mg). For this, preweighed amounts of SPI were added, separately, to 10 mL of 0.1 M NaOH solution and stirred for 60 min. All samples were adjusted to a pH of 2 ± 0.01 by adding 0.5 M HCl solution, followed by adding the Bradford reagent (0.3%) solution until the solutions turned blue. The SPI concentration of each solution was measured by UV/Vis spectrometer (Perkin-Elmer Lambda 35, Waltham, MA), with the absorbance peak at 595 nm.

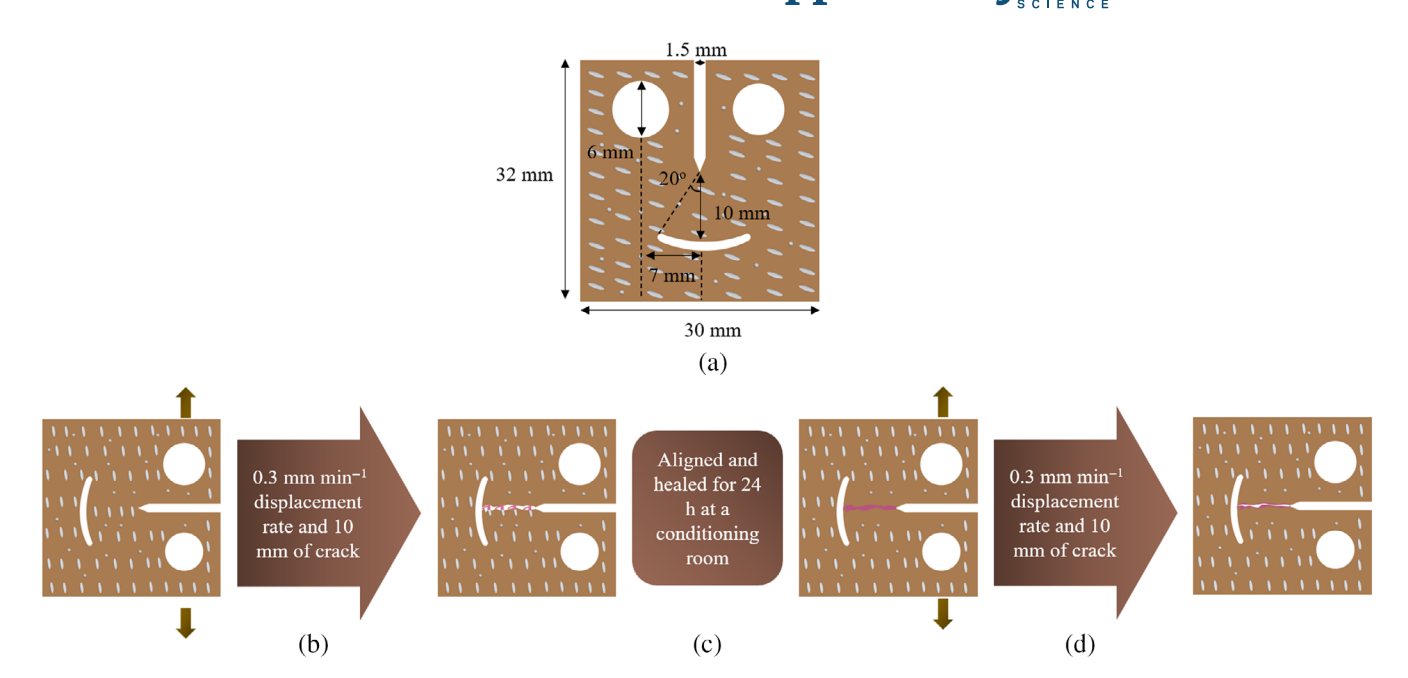


FIGURE 2 Schematic of the self-healing efficiency test (a) specimen dimensions, (b) fracture toughness testing on an MC-CA-SPI resin specimen, (c) healing at 65% RH and 21°C for 24 h, and (d) fracture toughness testing on the healed MC-CA-SPI resin specimen. CA, cinnamaldehyde; MC, microcapsule; SPI, soy protein isolate. [Color figure can be viewed at wileyonlinelibrary.com]

2.6 | Tensile characterization of CA-SPI resins

The conditioned CA-SPI resin sheets were laser cut to obtain the tensile specimens with dimensions of $70 \text{ mm} \times 5 \text{ mm} \times 2 \text{ mm}$. Pure SPI and CA-SPI specimens were characterized for their tensile properties according to ASTM D882-02 standard using strain rate of 0.067 min⁻¹ and gauge length of 30 mm.⁵⁴ All samples were tested on an Instron universal tensile tester (Instron) in triplicate (Instron, Model 5566, Instron Co, Canton, MA) to ascertain the reproducibility and obtain average values and standard deviations for statistical analyses.

2.7 | Determination of self-healing efficiency of MC-CA-SPI resins

Figure 2 shows various steps involved in the self-healing test. The conditioned MC-CA-SPI resin sheets were laser-cut to the final dimensions of 32 mm × 30 mm × 2 mm, as shown in Figure 2a, as per ASTM E647-08, with slight modification. At 10 mm below the precrack tip, a 40-deg arc was also laser cut. The purpose of including the arc was to capture and arrest the cracks from propagating further than 10 mm during the self-healing test. Using the same Instron, all self-healing specimens were pulled apart at a 0.3 mm min⁻¹ displacement rate until the specimen crack propagated 10 mm to reach the arc,

as shown in Figure 2b. At that point, the Instron was automatically set to return to its original position. The two fractured halves of the specimen were held together and allowed to heal in the conditioning room maintained at the ASTM conditions of 21°C and 65% RH for 24 h, as shown in Figure 2c. After 24 h, the crack propagation test with the exact Instron settings was rerun again on the control and the healed specimens to assess the healing efficiency, as shown in Figure 2d. Each sample category was prepared and tested in triplicate to confirm the reproducibility and to obtain average values and standard deviations. The self-healing efficiency of each MC loaded resin was calculated in terms of both strength (load at break) and toughness (areas under the curve in the load-displacement plots) using the following formulae⁵⁶:

$$\eta_P = \frac{P_{\text{healed}}}{P_{\text{virgin}}} \times 100,$$
(1)

$$\eta_T = \frac{T_{\text{healed}}}{T_{\text{virgin}}} \times 100,$$
(2)

where η_P is the crack healing efficiency in terms of strength, η_T is the crack healing efficiency in terms of toughness, P_{virgin} is the peak fracture load of the virgin specimens, P_{healed} is the peak fracture load of the healed specimens after 24 h, T_{virgin} is fracture toughness (area under the curve) of the virgin specimens, and T_{healed} is fracture toughness of the healed specimens after 24 h.

10974268, 0, Downloaded from https://onlinelibrary.wiley.com/doi/10.1002/app.53324 by Comell University Library, Wiley Online Library for rules of use; OA articles are governed by the applicable Creative Commons License

(c)
$$+ 2$$
 $+ 2$ $+ 10$

FIGURE 3 Three possible reaction mechanisms of crosslinking proteins with cinnamaldehyde (CA) via (a) Schiff base formation between CA and a primary amine, (b) nucleophilic attack on the β -unsaturated carbon via a 1,4-Michael addition reaction, and (c) phenol groups and CA. ²⁸

2.8 | Statistical analysis

Statistical analysis of the effect of CA on the mechanical properties of the SPI-based resins and the effect of MC loading on the self-healing efficiency of the resins was performed using the one-way analysis of variance (ANOVA) followed by multiple comparison tests using Tukey–Kramer's HSD at 95% confidence level. All analyses were carried out using Origin software (OriginLab Corporation, Northampton, MA).

3 | RESULTS AND DISCUSSION

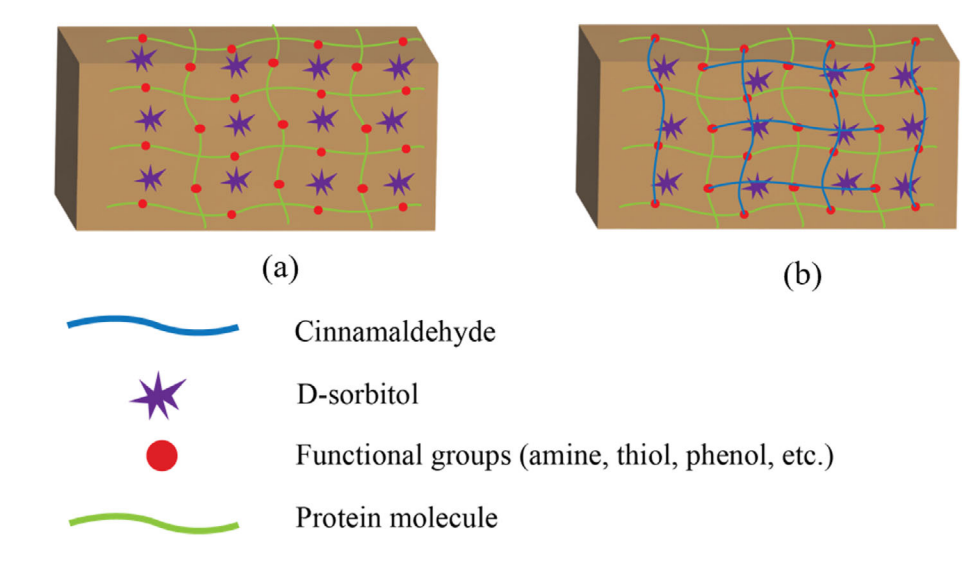
3.1 | Cinnamaldehyde crosslinked SPI (CA-SPI) resin

3.1.1 | Effect of cinnamaldehyde on the tensile properties of CA-SPI resin

Pure SPI resin sheets without plasticizers are very brittle and difficult to hot-press.²⁸ As a result, plasticizers, such

as D-sorbitol, are often used to increase their compliance, toughness, and ductility.⁵⁷ However, excessive sorbitol can make the SPI resins weak and susceptible to moisture absorption, which reduces their strength further. Mechanical properties and moisture resistance of SPI resins can be significantly improved via crosslinking using green crosslinkers such as CA.²⁸ Figure 3 shows three possible covalent crosslinking mechanisms of CA and proteins: Schiff base formation, Michael addition, and phenol-aldehyde condensation.²⁸ Since CA contains two electrophilic sites (the carbonyl and the β -carbon), theoretically, CA can react with nucleophilic groups (i.e., amine groups of lysine residues via Schiff base formation or thiol groups of cysteine via Michael addition).⁵⁸ Because of the presence of aldehyde groups in CA, some researchers have utilized CA as the crosslinking agent to make gels and films.⁵⁹ In the case of soy proteins, the aldehyde group of CA can react with the phenol group of tyrosine to form crosslinked protein networks. 28,60 Figure 4 shows the schematic of plasticized SPI resins, where D-sorbitol molecules appear embedded between protein chains (a), and the diagram of the

FIGURE 4 Schematic of an soy protein isolate (SPI) resin with (a) D-sorbitol plasticizers and (b) D-sorbitol plasticizers and cinnamaldehyde crosslinked protein molecules. [Color figure can be viewed at wileyonlinelibrary.com]



crosslinked SPI resins, where CA molecules form 3D networks with the protein molecules (b).

To study the effect of CA crosslinking, SPI resin with 10% (w/w) sorbitol was chosen as the control for the noncrosslinked resin and various amounts of CA, up to 10% (w/w), were added to crosslink the soy protein molecules. All resin specimens were tensile tested as per ASTM D882-02. Figure 5 shows typical stress-strain plots for control and crosslinked SPI resin specimens as a function of CA concentration, and Figure 6 shows calculated Young's modulus, tensile strength, fracture strain, and toughness values. It can be seen from Figure 5 that the plasticized SPI resins (control), as expected, behaved in a ductile manner, with high fracture strain of 43%, high toughness (area under the curve) of 7.15 MPa, low tensile strength of 15 MPa, and low Young's modulus of 423 MPa. Crosslinking SPI with 10% CA, increased the tensile strength of the resin by about 87% (from 15 to 28 MPa), and Young's modulus by 54% (423 to 652 MPa). In addition, as expected, there was a decrease in fracture strain, which in turn, reduced the toughness, particularly when 8% or more of CA was added. Fracture strain and toughness decreased by 85% and 87%, respectively, after adding 8% CA. The 10%CA-SPI resin, with higher crosslinking, exhibited low fracture strain of just 3.3% and low toughness of 0.49 MPa, indicating brittle behavior. ANOVA results confirmed that differences in all tensile properties between the control and 8%CA-SPI and 10% CA-SPI resins (p-value <0.05) are significant. When comparing the tensile properties of control resin with those of 5%CA-SPI resins, there was no significant difference in tensile strength, fracture strain, and toughness (p-value >0.05) while the difference in Young's modulus was significant (p-value <0.05). From these results it can be concluded that the effect of CA on SPI resins is significant only for higher (above 8%) content of CA. At low CA

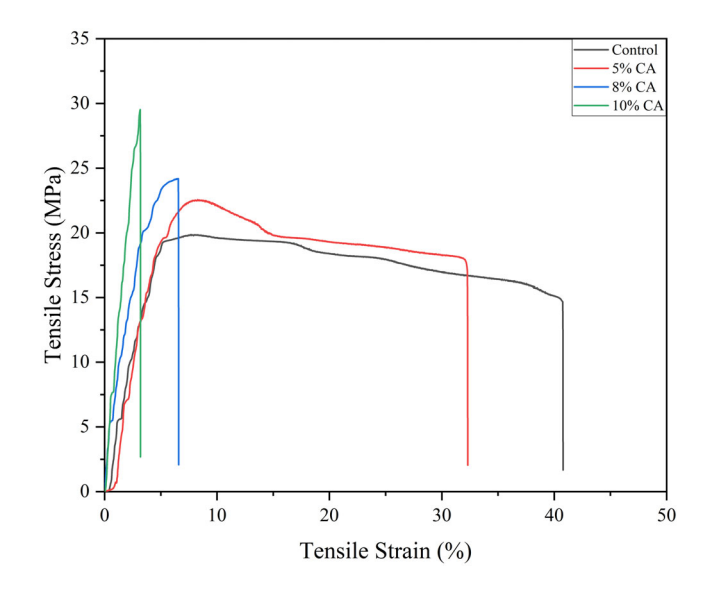


FIGURE 5 Stress-strain curve for the control and cinnamaldehyde crosslinked soy protein isolate sheets. CA, cinnamaldehyde. [Color figure can be viewed at wileyonlinelibrary.com]

content the crosslink density is not high enough to make a difference in the tensile properties.

The fracture behavior of the resins during tensile failure was characterized through SEM images of the fracture surfaces of the specimens. Figure 7a,b shows SEM images of control (0%CA-SPI specimens with 10% sorbitol) and 5% CA-SPI specimens (10% sorbitol). Both exhibit ductile behavior, indicated by the well-developed spurs and dimples that look similar to those of ductile metals and plasticized resins such as epoxies. However, for specimens crosslinked with 8% and 10% CA (Figure 7c,d), the fracture surfaces were much smoother and had less presence of voids and porosities similar to brittle epoxies. At 10% CA, the resin is very brittle. Noticeable river flow-like patterns

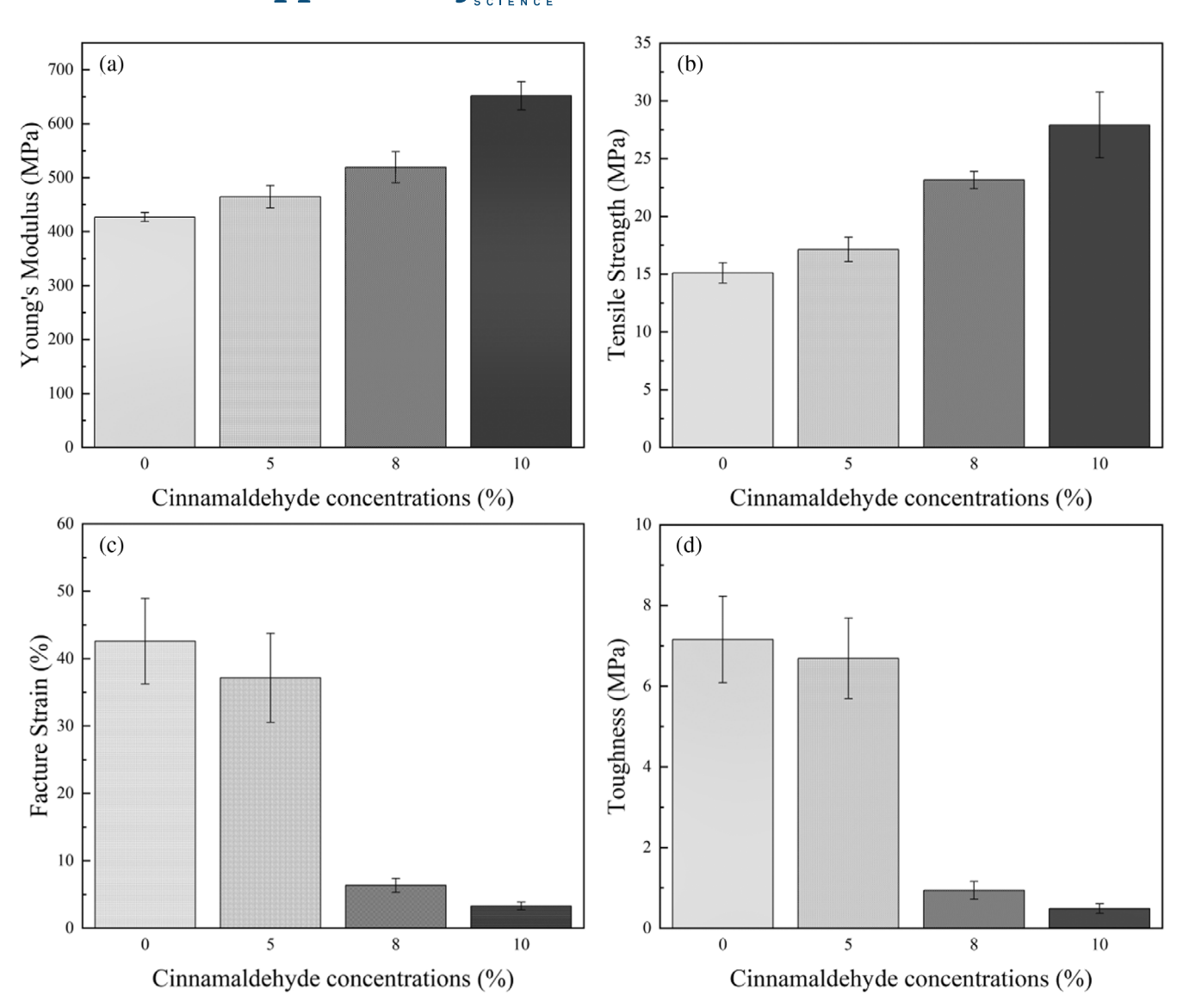


FIGURE 6 Effect of cinnamaldehyde (CA) on the tensile properties of CA-SPI resin sheets: (a) Young's modulus, (b) Tensile Strength, (c) Fracture strain, and (d) Toughness of SPI sheets as a function of CA contents. SPI, soy protein isolate.

and cracks in these specimens indicate the brittle nature and weak resistance to crack initiation and propagation. The brittle behavior that displays susceptibility to cracks and microcracks made 10%CA-SPI resins the best candidate for the self-healing efficiency assessment and was selected for this study.

3.2 | Elongated microcapsules

Successful fabrication of elongated MCs via ESE method can be attributed to several factors, including stirring speeds during emulsification, concentration of surfactant PVA in the aqueous phase, concentration of surface-active molecules such as sodium tripolyphosphate (STP) in the aqueous phase, and the viscosity of the core material (SPI, healing agent). The emulsification speed

influences the droplet dynamics as increase in stirring rate increases the shear forces acting on the droplets, stretching them. PVA, acting as an emulsion stabilizer, coats the droplet surfaces to provide an energy barrier that reduces coalescing of colliding droplets. ⁶² The surface-active agent lowers the oil-aqueous interfacial tension in the ESE method and, thus, favors droplet deformation. ⁶³ Effect of PVA and STP concentrations on microcapsule deformation is discussed below.

3.2.1 | Effect of PVA concentration in the aqueous phase on MC shape

PVA is a known emulsion stabilizer for PLGA particles.⁶⁴ To study the effect of PVA on particle deformation, the concentration of PVA was varied from 0.5% to 5.0% (w/v)

10974628, 0, Downloaded from https://onlinelibrary.wiley.com/doi/10.1002/app.55324 by Comell University Library, Wiley Online Library on [25/03/2024]. See the Terms

mditions) on Wiley Online Library for rules of use; OA articles are governed by the applicable Creative Commons

FIGURE 7 Scanning electron microscope images of fracture surface of (a) 0%CA-SPI, (b) 5%CA-SPI, (c) 8%CA-SPI, and (d) 10%CA-SPI. CA, cinnamaldehyde; SPI, soy protein isolate. [Color figure can be viewed at wileyonlinelibrary.com]

while keeping STP concentration at 0.04 M. Figure 8 shows SEM images of MCs fabricated at various PVA concentrations. It is clear that porosities and voids do develop at multiple locations on the microcapsule surface when less PVA is present. At 0.5% and 1% PVA, some MCs were broken due to insufficient amount of the emulsifier while others were stretched with an extremely jagged and porous surface, as can be seen in Figure 8a,b, respectively. In addition, compared with the MCs obtained with 0.5% PVA, elongated MCs fabricated with 1% PVA had smoother surfaces and were smaller in diameter. At 2% PVA, the emulsifier helps maintain the stability of the w/o (PLGA-SPI) emulsion and allows formation of smooth elongated MCs as seen in Figure 8c. Above 2% PVA, the aspect ratio of the particles decreased, suggesting that smaller MCs become stable and reach the upper limit of PVA concentration that favors elongated MC formation. The conventional magnetic stirrer at fixed 700 rpm did not create enough shear

force to deform the emulsion droplets, perhaps due to the highly viscous aqueous solution (5.0% PVA). Instead, large emulsion droplets underwent multiple breaks and eventually formed tiny droplets, as shown in Figure 8d. As a result, the PVA concentration was fixed at a concentration of 2.0%.

3.2.2 | Effect of STP concentration in the aqueous phase on MC shape

Many earlier studies have used tris base (Trizma),^{52,63} phosphate buffer saline,⁵¹ or STP^{53,65} to initiate the deformation of emulsion droplets. In the present study, PVA concentration in the aqueous phase was held constant at 2.0% (w/v), and STP concentrations from 0 M to 0.06 M were introduced to the PVA aqueous phase to investigate the degree of emulsion deformation, which was quantified by the aspect ratio of the particles. Figure 9 presents

FIGURE 8 Scanning electron microscope images of MCs fabricated at various concentrations of PVA: (a) 0.5%, (b) 1.0%, (c) 2.0%, and (d) 5.0% (w/v) PVA, at fixed 0.04 M STP and 700 rpm stirring rate. MCs, microcapsules; PVA, poly(vinyl alcohol); STP, sodium tripolyphosphate.

SEM images of MCs fabricated at various STP concentrations. As expected, SEM image for 0 M STP shown in Figure 9a, indicates no sign of MC deformation as most MCs retained their spherical shape. However, upon increasing the STP concentration to 0.02 M, although some MCs were stretched, most were predominantly spherical with an average diameter of less than 1 µm, as can be seen in Figure 9b. At 0.04 M STP, most of the MCs were elongated with smooth and well-defined shell. Figure 9c reveals the appearance of elongated MCs at the optimal conditions of 2% (w/v) PVA, 0.04 M STP, and 700 rpm stirring rate. Figure 10 presents the SEM image of elongated MCs and the histograms of their dimensions and aspect ratios. SEM image of the MCs is presented in Figure 10a. Histograms of MC length and width (diameter) (N > 100) are shown in Figure 10b,c, respectively. The calculated average length and width values were 13.2 and 3.14 µm with standard deviations (SD) of 6.24 and

0.65 μm, respectively. The histogram of MC aspect ratios (AR) is presented in Figure 10d. The average AR value was 4.04 with SD of 1.74. In addition, about 60% of the elongated MCs had ARs between four and six.

Following the protocol developed earlier by Kim and Netravali,² encapsulation efficiency and protein loading of microcapsules fabricated under the optimal conditions were 55% and 68%, respectively. It was noticed that as STP concentration was raised to above 0.04 M, a considerable amount of PVA gel was formed, making it difficult to fabricate elongated MCs.

Confocal laser scanning microscopy 3.2.3 analysis

Encapsulated SPI resin content and structure of the MCs were confirmed via CLSM. Figure 11 shows the well-

.0974628, 0, Downloaded from https://onlinelibrary.wiley.com/doi/10.1002/app.55324 by Comell University Library, Wiley Online Library on [25/03/2024]. See the Terms and Condition

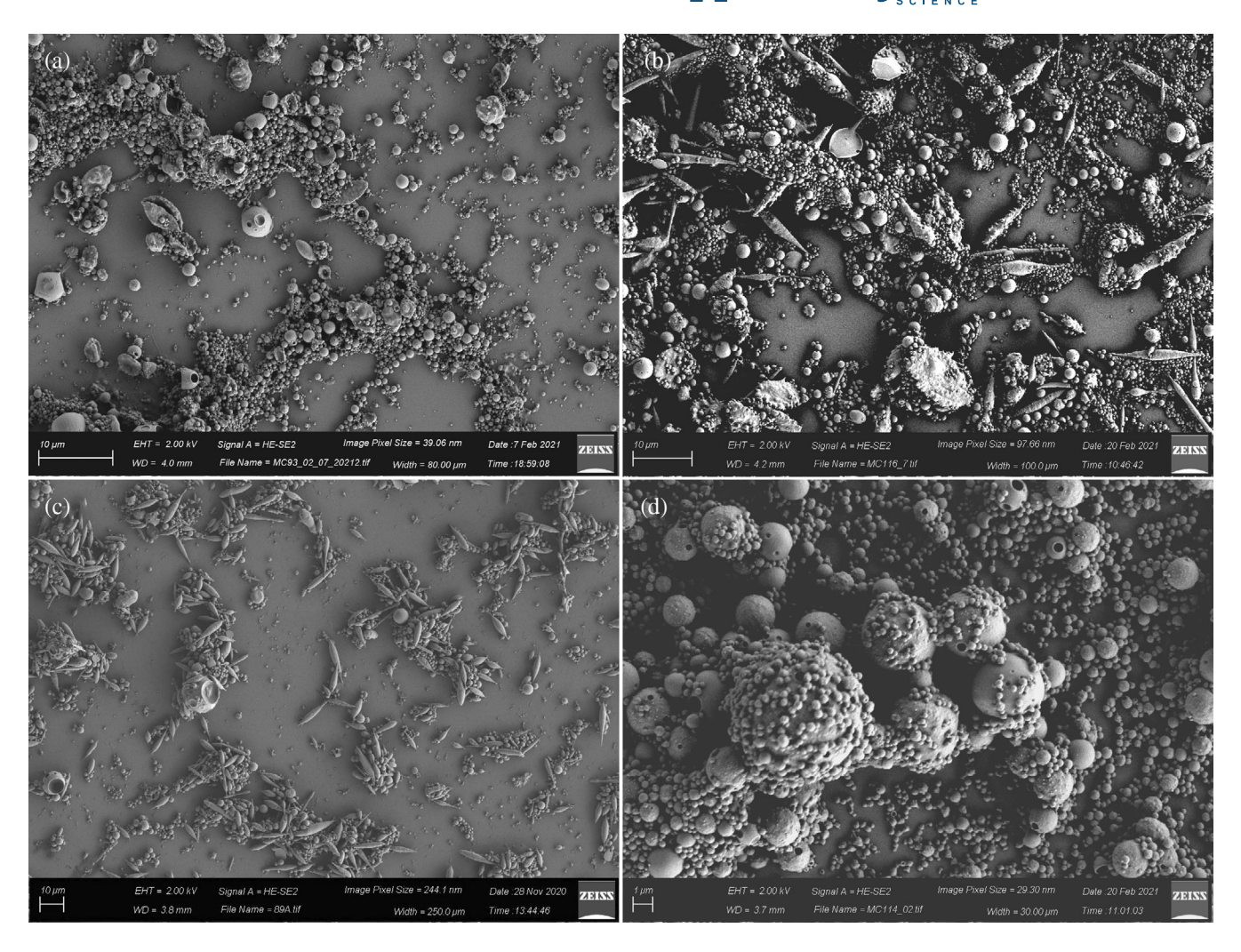


FIGURE 9 Scanning electron microscope images of microcapsules (MCs) fabricated at various sodium tripolyphosphate concentrations: (a) 0.00 M, (b) 0.02 M, (c) 0.04 M, and (d) 0.06 M, at fixed 2% (w/v) poly(vinyl alcohol) and stirring rate of 700 rpm.

defined shapes of elongated MCs and the core-shell structure via the overlay of transmission and fluorescent images. The bright red fluorescent signal indicates the presence of SPI resin inside the MCs. As mentioned earlier, the protein was stained with Rhodamine B. Figure 12 shows the CLSM image of elongated MCs with holes and sub-capsules at higher magnification. Multiple discrete subcapsules and holes can be observed as bright red and black circles within the MCs. Holes can occur near the edges of MCs due to the small shell thickness. Such MCs do not retain the healant and, hence, are not preferred.

3.2.4 | ATR-FTIR analysis

Figure 13 shows the ATR-FTIR spectra of pure PVA, PLGA, SPI, and MCs. The ATR-FTIR spectrum of PVA shows a broad peak for O—H stretching vibration at

3290 cm⁻¹, C—H symmetrical and asymmetrical stretching at 2910 and 2940 cm⁻¹, and C—O stretching at 1090 cm⁻¹.⁶⁶ The ATR-FTIR spectrum of PLGA shows sharp peaks at 1750 and 1080 cm⁻¹ for (—C=O) and (—C—O—C—), respectively.^{67,68} For pure SPI, the amine (—NH₂) peaks resulting from amino acids such as lysine and arginine can be seen between 1550 and 1650 cm⁻¹.^{14,69} ATR-FTIR spectrum of MC shows the presence of PVA, PLGA, and SPI via O—H and C—O peaks of PVA, C=O carbonyl and C—O—C peaks of PLGA, and the NH₂ peak of SPI. From these spectra, it can be concluded that PLGA, PVA, and SPI residues exist on the MC surfaces.

3.3 | Self-healing efficiency of SPI resins

Figure 14 shows the effect of elongated MCs loading on the 10%CA-SPI resin failure load during the self-healing

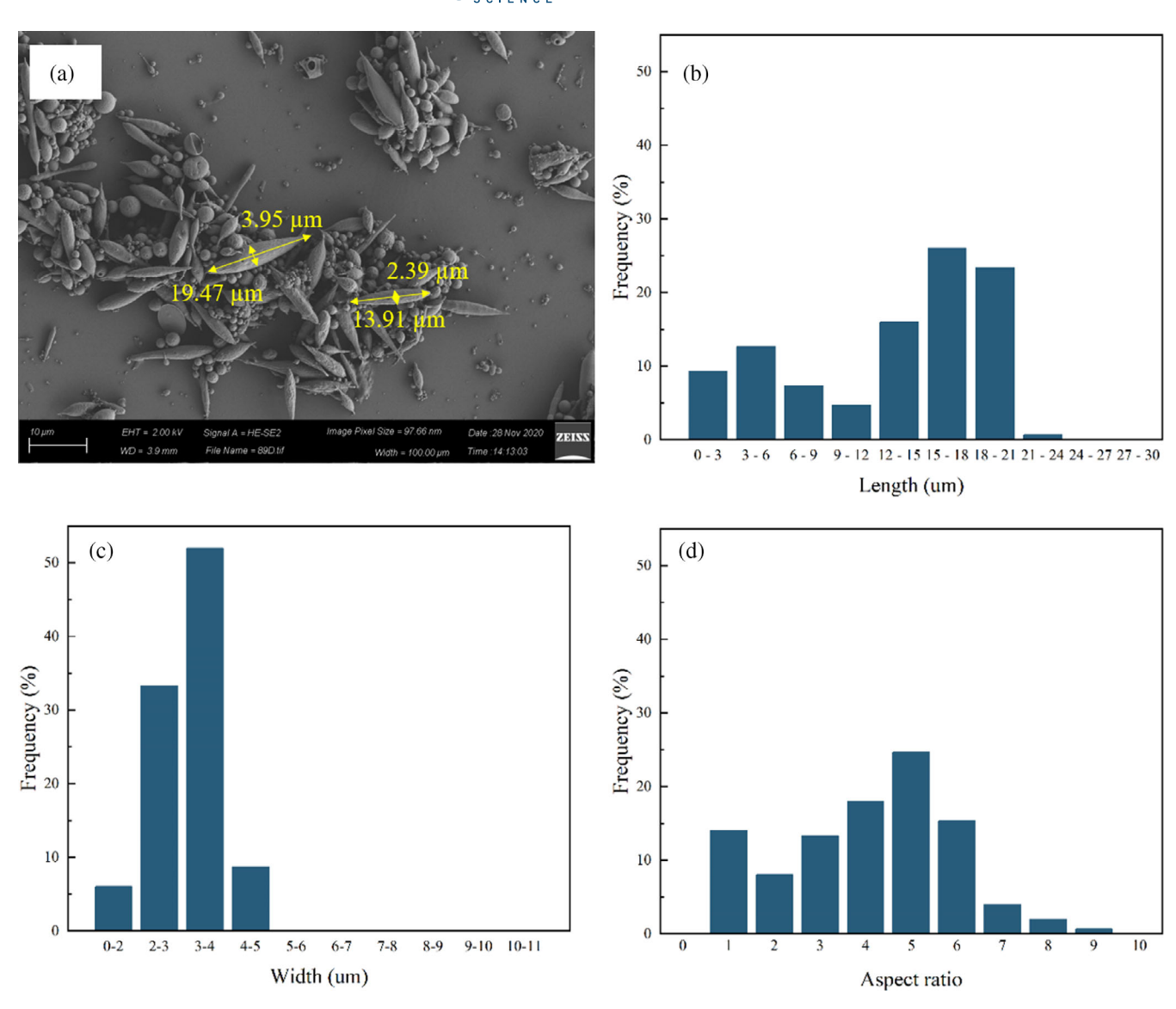


FIGURE 10 Details of microcapsules (MCs), fabricated at 2% poly(vinyl alcohol), 0.04 M STP, and 700 rpm stirring rate: (a) scanning electron microscope image of elongated MCs, and histograms of MC (b) lengths, (c) widths (diameters), and (d) aspect ratios. [Color figure can be viewed at wileyonlinelibrary.com]

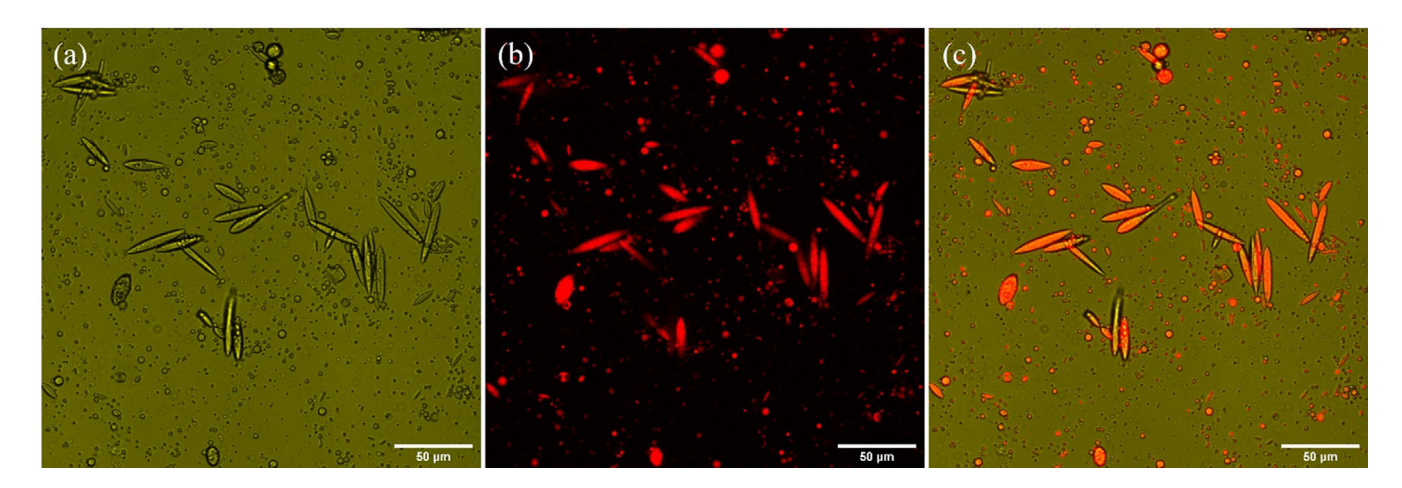


FIGURE 11 Confocal laser scanning microscopy images of elongated microcapsules: (a) transmission image, (b) fluorescent image, and (c) overlay of the transmission and fluorescent image. [Color figure can be viewed at wileyonlinelibrary.com]

and-conditions) on Wiley Online Library for rules

of use; OA articles are governed by the applicable Creative Comn

efficiency tests. Figure 14a shows typical load-displacement plots for 10%CA-SPI resin specimens containing various MC loadings (0%, 5%, 10%, and 15%) as virgin and 24 h healed. Figure 14b shows histograms of the peak fracture loads of the virgin resins and the healed

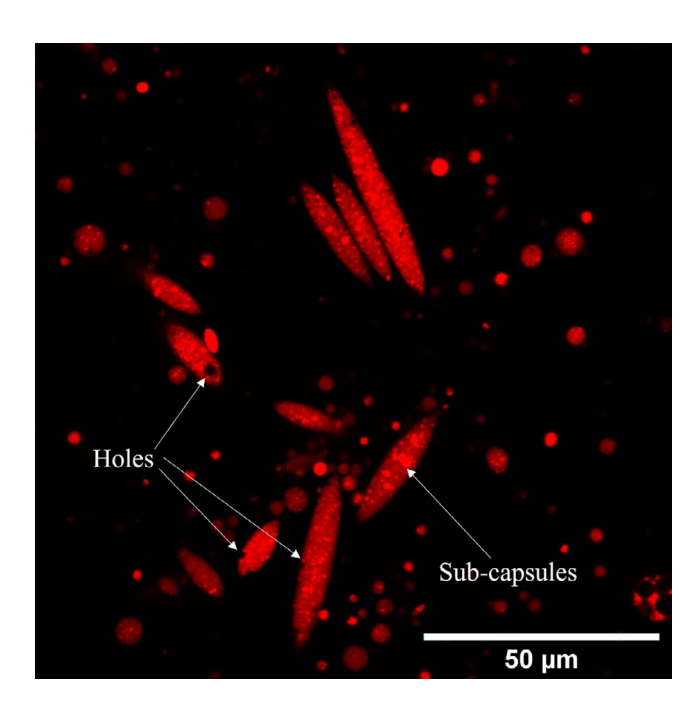
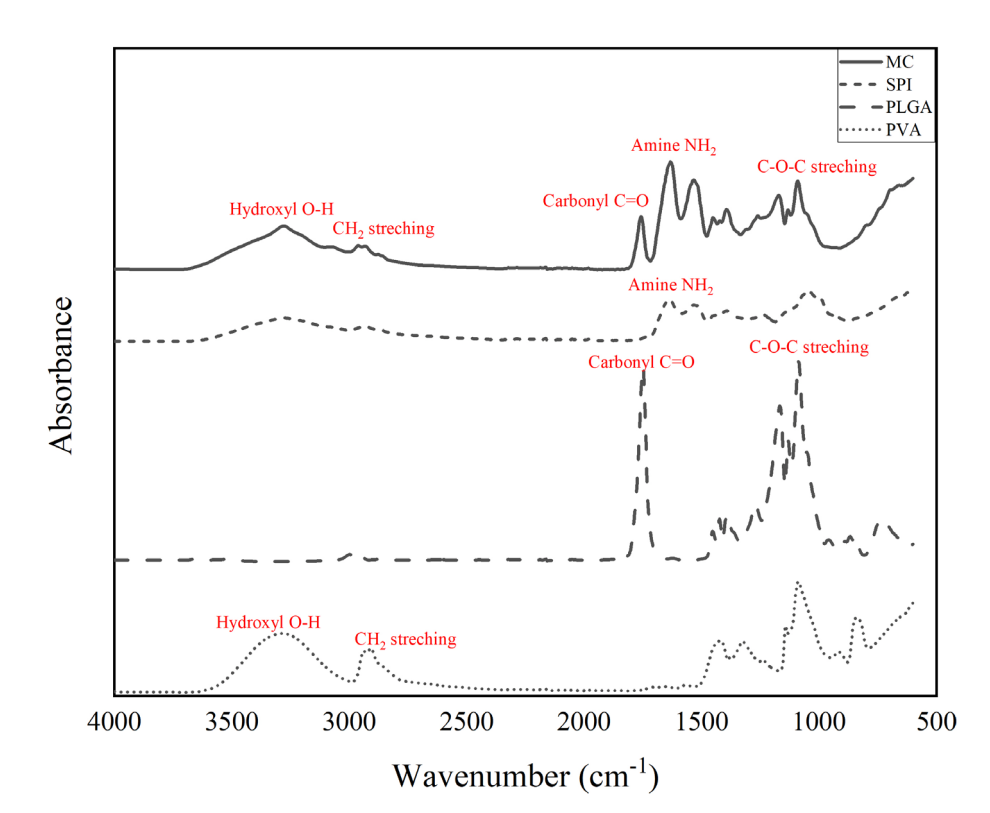


FIGURE 12 Confocal laser scanning microscopy image of elongated microcapsules (MCs) with holes and subcapsules. [Color figure can be viewed at wileyonlinelibrary.com]

resins as well as their self-healing efficiencies in terms of fracture strength. Figure 14c shows histograms of the fracture toughness of the virgin and the healed resins as well as their self-healing efficiencies in terms of fracture toughness. Compared with the MC-loaded resins, the 0% MC-10%CA-SPI resins show a negligible self-healing efficiency of just 1.4%, as shown in Figure 14b. After incorporating elongated MCs, the resins exhibited a significant increase in the self-healing efficiency, in strength, of 42.7% for 15%MC-10%CA-SPI resins (*p*-value <0.05). When calculated in terms of toughness recovery, the selfhealing efficiency of the resins increased significantly from 1.3% for 0%MC-10%CA-SPI to 12.3% for 5%MC-10% CA-SPI and 35% for 15%MC-10%CA-SPI resin (p-value <0.05), as seen in Figure 14c. When microcracks start to grow, microcapsules in their path fracture releasing the healant, which fills the microcracks and bridges the surfaces as it gets cured within the 24 h healing period. The curing of healant (SPI) is facilitated by the additional crosslinking agent, CA, present in the surrounding resin. Figure 14d shows a typical fracture surface of the 15% MC-10%CA-SPI resin, where the broken elongated MCs appear as caterpillar-like structure against the smooth resin surface. Figure 15 illustrates the bridging zone in the resin containing 15% MC, where elongated MCs have broken in the crack path, releasing the SPI healant to form bridges between the fracture surfaces. Multiple imprints of elongated MCs are shown along the crack path, where the shells have been emptied of the healant.



reflectance Fourier-transform infrared spectra of poly(vinyl alcohol), poly(lactic-co-glycolic acid), soy protein isolate, and microcapsules. [Color figure can be viewed at wileyonlinelibrary.com]

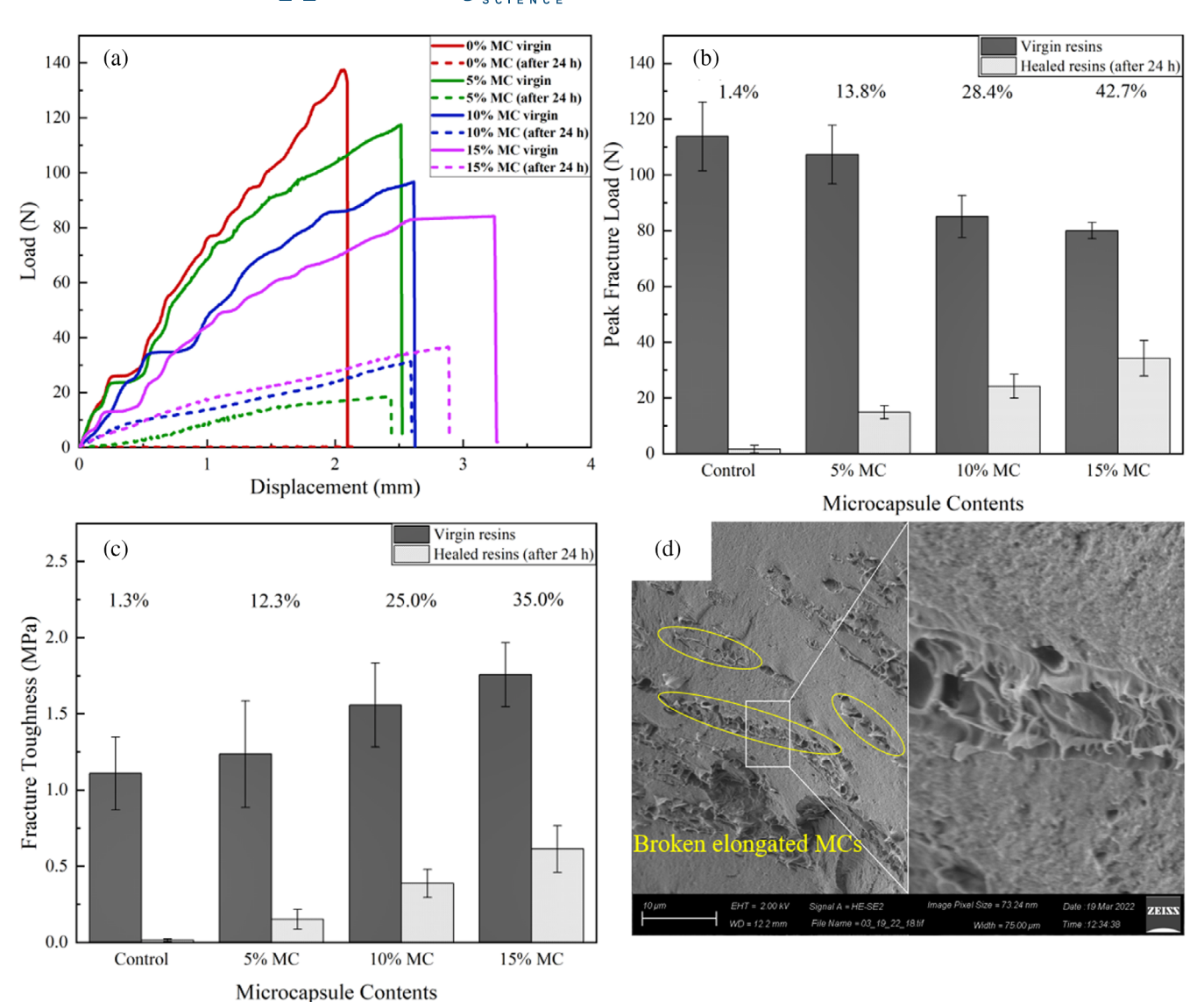
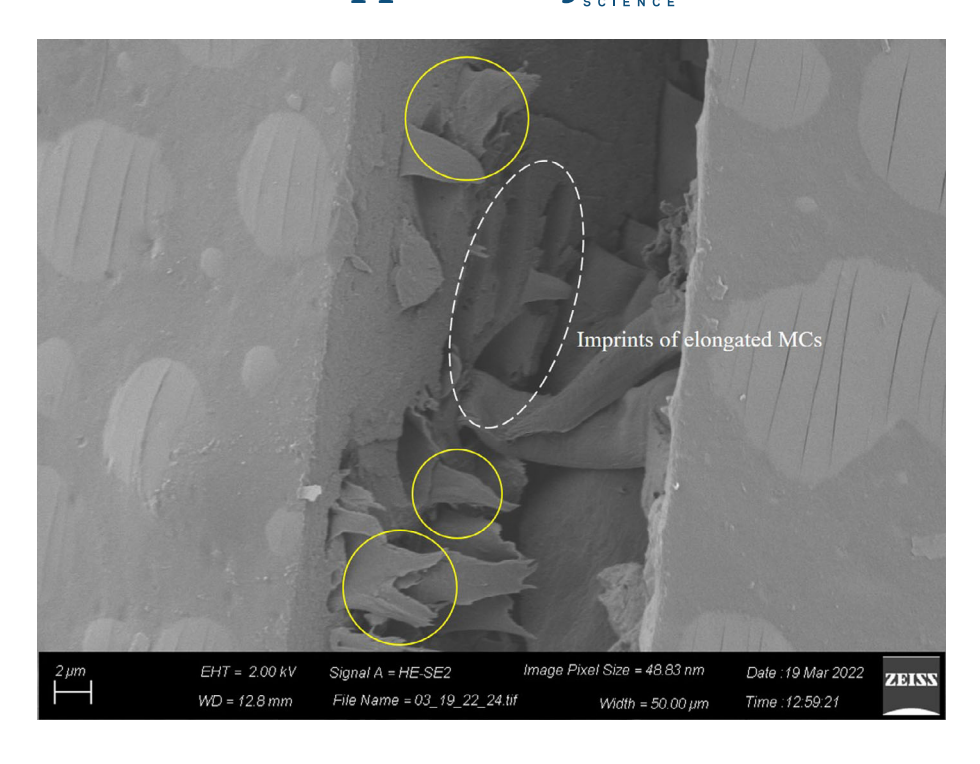


FIGURE 14 Self-healing test results: (a) Typical load—displacement plots of control (without microcapsule [MC]) and various MC-loaded and 24 h healed resin specimens. (b) Histograms of peak fracture loads of control and various MC-loaded and 24 h healed resin specimens and their self-healing efficiencies in terms of fracture strength. (c) Histograms of fracture toughness of various control and MC-loaded and 24 h healed resin specimens and their self-healing efficiencies in terms of fracture toughness.(d) scanning electron microscope images of the fracture surface of the 15%MC-10%CA-SPI specimen. CA, cinnamaldehyde; SPI, soy protein isolate. [Color figure can be viewed at wileyonlinelibrary.com]

It is clear from Figure 14a that adding more MCs in resins leads to lowering of resin tensile properties such as stiffness (modulus) and peak fracture load and increases the fracture strain. For example, the virgin 15%MC-10%CA-SPI resin has a peak fracture load of 84 N and the displacement at break of 3.25 mm, whereas the virgin 5%MC-10%CA-SPI resins has a higher peak fracture load of 119 N and the displacement at break of 2.52 mm. Similar observations were also made by earlier researchers. Another underlying consequence of adding MCs is the improvement in fracture toughness. Figure 14c shows that the fracture

toughness of the virgin resins increased steadily with MC loading. For example, fracture toughness increased from 1.11 MPa for 0%MC-10%CA-SPI resins to 1.55 MPa for 10%MC-10%CA-SPI resins and 1.76 MPa for 15%MC-10%CA-SPI resins. This is in agreement with the results obtained by earlier researchers. This toughening effect can be attributed to the increased fracture strains and the rubber-like deformations of the SPI slurry-filled soft MCs, when stressed. MCs may also add free volume to the resin system through the PVA present on their surfaces. This can reduce the glass transition temperature of the SPI resin and help reduce

reference in scanning electron microscope images of the bridging zone in 15%MC-10%CA-SPI, where SPI healant has oozed out of the elongated MCs and formed connecting bridges between the fracture surfaces. CA, cinnamaldehyde; MCs, microcapsules; SPI, soy protein isolate. [Color figure can be viewed at wileyonlinelibrary.com]



the stress concentration at the crack tips. The MC-induced plasticization effect, however, was not seen in healed resins. This may be attributed to the fact that during crack propagation testing post-self-healing, stresses are heavily concentrated at the bridged zones where the SPI healant bridges the microcrack. The bridged zone, however, is not perfectly healed and, hence, can fracture at lower stress than intact resin.

The healed resin specimens could only attain maximum self-healing efficiency 43% due to several factors. First, partially crosslinked SPI healant bridges are weak and can fracture easily compared to fully cured resins. Crosslinking the healant could improve its mechanical properties and, hence, the self-healing efficiency. Second, even with 15% MC loading there is insufficient amount of SPI healant to bridge large cracks. Some parts of the fracture surfaces are seen as smooth without any microcapsules or broken MCs, as seen in Figure 15. These areas did not have the healant to bridge the microcracks and thus had no contribution to the overall strength or toughness recovery. Last, whether the healant can flow and fill the crack depends on the orientation of elongated MCs in the resin relative to the crack path. Figure 16 shows a schematic of a scenario in which elongated MCs positioned at small angle with the crack path cannot contribute to healing. This is because when a crack propagates through the vertex of the MCs, only the tip of the shell gets ruptured. Since a significant part of the body remains embedded in the resin, a major portion of the healant remains trapped and cannot contribute to the healing process.

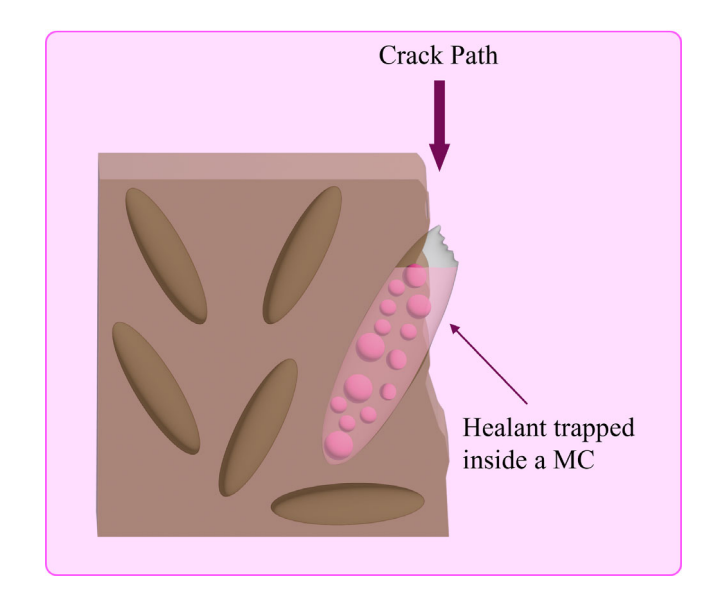


FIGURE 16 Schematic of a scenario in which the healant is trapped inside an elongated microcapsule (MC). [Color figure can be viewed at wileyonlinelibrary.com]

4 | CONCLUSIONS

The mechanical properties of crosslinked SPI resins with different amounts of CA (0% to 10% w/w of SPI) were studied. Parameters such as concentrations of PVA (0.5% to 5% w/v) and STP (0.00 M to 0.06 M), were investigated to determine the optimal concentrations of both to successfully obtain elongated MCs. 10%CA-SPI resins with various loadings of MCs (5%, 10%, and 15% w/w of SPI)

were prepared and characterized for their mechanical properties and self-healing efficiencies. The self-healing efficiencies in strength recovery varied from a low of 13.8% to a high of 42.7% and in toughness recovery from 12.3% to 35.0%, as CA% was increased to 10%.

Based on the overall results obtained from this study, the following conclusions can be made:

- 1. CA crosslinking enhanced the mechanical properties (Young's modulus and tensile strength) of the green thermoset SPI resins, with 8% CA being optimal.
- 2. Increasing PVA concentration led to better formation of MCs with less porosity since PVA acted as the emulsion stabilizer.
- 3. Elongated MCs were achieved by incorporating surfaceactive agent (STP) into PVA solution. The 0.04 M STP in 2% (w/v) PVA favored stable emulsion and MC deformation. However, STP concentration higher than 0.04 M led to formation of unworkable PVA gel.
- 4. The average aspect ratio of elongated MCs was just over four and about 60% of MCs had aspect ratios between four and six.
- 5. Incorporating elongated MCs into SPI resins improved fracture toughness of the SPI resin, possibly due to rubber-like deformation of soft MCs and the presence of PVA.
- 6. Healant released from fractured microcapsules was able to form connecting bridges within microcracks. This resulted in obtaining maximum self-healing efficiency of 42.7% in strength recovery and 35.0% in toughness recovery.

AUTHOR CONTRIBUTIONS

Vuthtyra Yong: Conceptualization (equal); investigation (lead); methodology (lead); writing – original draft (lead); writing – review and editing (supporting). **Anil Netravali:** Conceptualization (equal); project administration (lead); resources (lead); supervision (lead); writing – review and editing (lead).

ACKNOWLEDGMENTS

This work made use of the Cornell Center for Materials Research shared facilities, which are supported through the NSF MRSEC program (DMR-1719875). Laboratory facilities in the College of Human Ecology were also used.

FUNDING INFORMATION

This study was not funded by any grant.

CONFLICT OF INTEREST STATEMENT

The authors declare that they have no known competing financial interest or personal relationship that could have influenced the work reported in this paper.

DATA AVAILABILITY STATEMENT

The data that support the findings of this study are available on request from the corresponding author. The data are not publicly available due to privacy or ethical restrictions.

ORCID

Anil N. Netravali https://orcid.org/0000-0002-2391-7116

REFERENCES

- [1] J. R. Kim, A. N. Netravali, Compos. Sci. Technol. 2017, 143, 22.
- [2] J. R. Kim, A. N. Netravali, Adv. Funct. Mater. 2016, 26, 4786.
- [3] H. Souzandeh, A. N. Netravali, Compos. Sci. Technol. 2019, 183, 107831.
- [4] A. N. Netravali, X. Huang, K. Mizuta, Adv. Compos. Mater 2007, 16, 269.
- [5] R. Nakamura, A. N. Netravali, A. B. Morgan, M. R. Nyden, J. W. Gilman, Fire Mater. 2013, 37, 75.
- [6] R. Geyer, J. R. Jambeck, K. L. Law, Sci. Adv. 2017, 3, e1700782.
- [7] T. Reinhardt, U. Richers, H. Suchomel, Waste Manage. Res. 2008, 26, 88.
- [8] J. R. Kim, A. N. Netravali, Polymer 2017, 117, 150.
- [9] A. N. Netravali, S. Chabba, *Mater. Today* **2003**, *6*, 22.
- [10] P. Lodha, A. N. Netravali, Ind. Crops Prod. 2005, 21, 49.
- [11] A. Kamada, M. Rodriguez-Garcia, F. S. Ruggeri, Y. Shen, A. Levin, T. P. J. Knowles, *Nat. Commun.* 2021, 12, 1.
- [12] R. P. Wool, Soft Matter 2008, 4, 400.
- [13] R. O. Ritchie, Philos. Trans. A Math. Phys. Eng. Sci. 2021, 379, 20200437.
- [14] S. Shi, A. N. Netravali, J. Mater. Sci. 2021, 56, 12030.
- [15] S. Shi, A. N. Netravali, J. Polym. Environ. 2023, 31, 754.
- [16] A. Alkandary, A. N. Netravali, Composites, Part B 2023, 256, 110626.
- [17] K. Qiu, A. Netravali, Fibers 2017, 5, 31.
- [18] X. Huang, A. Netravali, Compos. Sci. Technol. 2009, 69, 1009.
- [19] P. Lodha, A. N. Netravali, Polym. Compos. 2005, 26, 647.
- [20] Q. Zhang, G. Xu, A. Pizzi, H. Lei, X. Xi, G. Du, *Polymer* 2022, 14. https://doi.org/10.3390/polym14142819
- [21] X. Xi, A. Pizzi, S. Amirou, Polymer 2018, 10. https://doi.org/10. 3390/polym10010022
- [22] M. Liu, Y. Wang, Y. Wu, Z. He, H. Wan, J. Cleaner Prod. 2018, 187, 361.
- [23] L. Cao, A. Pizzi, Q. Zhang, H. Tian, H. Lei, X. Xi, G. Du, Eur. Polym. J. 2022, 162, 110915.
- [24] Y. Xie, Z. Xiao, T. Gruneberg, H. Militz, C. A. S. Hill, L. Steuernagel, C. Mai, Compos. Sci. Technol. 2003, 2003, 70.
- [25] S. Chabba, A. N. Netravali, J. Mater. Sci. 2005, 40, 6263.
- [26] I. Paetau, C.-Z. Chen, J. Jane, J. Environ. Polym. Degrad. 1994, 2, 211.
- [27] M. P. Balaguer, J. Gómez-Estaca, R. Gavara, P. Hernandez-Munoz, J. Agric. Food Chem. 2011, 59, 6689.
- [28] M. M. Rahman, A. N. Netravali, ACS Sustainable Chem. Eng. 2014, 2, 2318.
- [29] Y. M. Malinskii, V. V. Prokopenko, N. A. Ivanova, V. S. Kargin, *Polym. Mech.* **1970**, *6*, 382.
- [30] D. Jayabalakrishnan, D. B. NagaMuruga, K. Bhaskar, P. Pavan, K. Balaji, P. S. Rajakumar, C. Priya, R. A. B. Deepa, S. Sendilvelan, M. Prabhahar, *Mater. Today: Proc.* 2021, 45, 7195.

of use; OA articles

- [31] A. A. Kavitha, N. K. Singha, ACS Appl. Mater. Interfaces 2009, 1, 1427.
- [32] K. S. Toohey, N. R. Sottos, J. A. Lewis, J. S. Moore, S. R. White, *Nat. Mater.* 2007, 6, 581.
- [33] Z. Xie, B.-L. Hu, R.-W. Li, Q. Zhang, ACS Omega 2021, 6, 9319
- [34] Y. Yang, X. Ding, M. W. Urban, Prog. Polym. Sci. 2015, 49–50, 34.
- [35] T. S. Coope, U. F. J. Mayer, D. F. Wass, R. S. Trask, I. P. Bond, Adv. Funct. Mater. 2011, 21, 4624.
- [36] A. R. Jones, A. Cintora, S. R. White, N. R. Sottos, ACS Appl. Mater. Interfaces 2014, 6, 6033.
- [37] L. Yuan, G. Liang, J. Xie, L. Li, J. Guo, *Polymer* **2006**, *47*, 5338.
- [38] D. Sun, H. Zhang, X.-Z. Tang, J. Yang, Polymer 2016, 91, 33.
- [39] J. T. Wertz, T. C. Mauldin, D. J. Boday, ACS Appl. Mater. Interfaces 2014, 6, 8511.
- [40] S. H. Cho, H. M. Andersson, S. R. White, N. R. Sottos, P. V. Braun, Adv. Mater. 2006, 18, 997.
- [41] C. L. Mangun, A. C. Mader, N. R. Sottos, S. R. White, *Polymer* 2010, 51, 4063.
- [42] L. M. Meng, Y. C. Yuan, M. Z. Rong, M. Q. Zhang, J. Mater. Chem. 2010, 20, 6030.
- [43] D. Y. Zhu, B. Wetzel, A. Noll, M. Z. Rong, M. Q. Zhang, J. Mater. Chem. A 2013, 24, 7191.
- [44] S. R. White, N. R. Sottos, P. H. Geubelle, J. S. Moore, M. R. Kessler, S. R. Sriram, E. N. Brown, S. Viswanathan, *Nature* 2001, 409, 794.
- [45] J. Yang, M. W. Keller, J. S. Moore, S. R. White, N. R. Sottos, *Macromolecules* 2008, 41, 9650.
- [46] J. R. Kim, A. N. Netravali, J. Mater. Sci. 2017, 52, 3028.
- [47] J.-M. Williford, J. L. Santos, R. Shyam, H.-Q. Mao, *Biomater. Sci.* 2015, 3, 894.
- [48] S. E. A. Gratton, P. D. Pohlhaus, J. Lee, J. Guo, M. J. Cho, J. M. DeSimone, J. Controlled Release 2007, 121, 10.
- [49] J. P. Rolland, B. W. Maynor, L. E. Euliss, A. E. Exner, G. M. Denison, J. M. DeSimone, J. Am. Chem. Soc. 2005, 127, 10096.
- [50] S. Xu, Z. Nie, M. Seo, P. Lewis, E. Kumacheva, H. A. Stone, P. Garstecki, D. B. Weibel, I. Gitlin, G. M. Whitesides, Am. Ethnol. 2005, 117, 734.
- [51] Q. Fan, F. Qi, C. Miao, H. Yue, F. Gog, J. Wu, G. Ma, Z. Su, Colloids Surf., A 2016, 500, 177.
- [52] M. J. Heslinga, E. M. Mastria, O. Eniola-Adefeso, J. Controlled Release 2009, 138, 235.

- [53] H. Safari, R. Adili, M. Holinstat, O. Eniola-Adefeso, J. Colloid Interface Sci. 2018, 518, 174.
- [54] Standard Test Method for Tensile Properties of Thin Plastic Sheeting. https://www.astm.org/d0882-02.html (accessed: May 18, 2022).
- [55] Standard Test Method for Measurement of Fatigue Crack Growth Rates. https://www.astm.org/e0647-00.html (accessed: May 17, 2022).
- [56] E. N. Brown, N. R. Sottos, S. R. White, Exp. Mech. 2002, 42, 372.
- [57] J. K. Sears, J. R. Darby, The Technology of Plasticizers, Wiley Publishers, Hoboken, NJ 1982, p. 35.
- [58] V. A. Majeti, R. R. Suskind, Contact Dermatitis 1977, 3, 16.
- [59] E. Chen, L. Cao, D. J. McClements, S. Liu, B. Li, Y. Li, Food Hydrocolloids 2018, 77, 976.
- [60] T. G. Dastidar, A. N. Netravali, Green Chem. 2013, 15, 3243.
- [61] A. N. Netravali, R. B. Henstenburg, S. L. Phoenix, P. Schwartz, Polym. Compos. 1989, 10, 226.
- [62] L. R. Fisher, N. S. Parker, CSIRO Food Res. Q. 1985. (accessed: Apr 13, 2022).
- [63] M. J. Heslinga, G. M. Willis, D. J. Sobczynski, A. J. Thompson, O. Eniola-Adefeso, *Colloids Surf.*, B 2014, 116, 55.
- [64] F. Qi, J. Wu, Q. Fan, F. He, G. Tian, T. Yang, G. Ma, Z. Su, Colloids Surf., B 2013, 112, 492.
- [65] R. Li, X. Li, L. Liu, Z. Zhou, H. Tang, Q. Zhang, Macromol. Rapid Commun. 2010, 31, 1981.
- [66] C.-P. Liu, C.-A. Dai, C.-Y. Chao, S.-J. Chang, J. Power Sources 2014, 249, 285.
- [67] B. Lu, X. Lv, Y. Le, Polymer 2019, 11, 304.
- [68] N. Thanki Paragkumar, D. Edith, S. Jean-Luc, Appl. Surf. Sci. 2006, 253, 2758.
- [69] N. V. Patil, A. N. Netravali, ACS Omega 2019, 4, 5392.
- [70] M. Kosarli, D. G. Bekas, K. Tsirka, D. Baltzis, D. T. Vaimakis-Tsogkas, S. Orfanidis, G. Papavassiliou, A. S. Paipetis, *Composites, Part B* 2019, 171, 78.

How to cite this article: V. Yong, A. N. Netravali, *J. Appl. Polym. Sci.* **2024**, e55324. https://doi.org/10.1002/app.55324